(Received 2 August 2025, Accepted 22 October 2025, Scheduled 5 November 2025)

Miniaturized Ultrawideband Circularly Polarized Antenna with Enhanced Axial Ratio Bandwidth for C-Band Automotive and Satellite Applications

Sanjeev Sharma[1], Ashish Kumar[2], Rajeev Kumar[2], Nitin K. Saluja[2], Zahriladha Zakaria[3], and Ahmed J. A. Al-Gburi[3,*]

[1]*Research Department, Rayat Bahra University, Mohali 140104, Punjab, India*
[2]*Chitkara University Institute of Engineering and Technology, Chitkara University, Punjab, India*
[3]*Center for Telecommunication Research & Innovation (CeTRI)*
Fakulti Teknologi Dan Kejuruteraan Elektronik Dan Komputer (FTKEK)
Universiti Teknikal Malaysia Melaka (UTeM), Jalan Hang Tuah Jaya, Durian Tunggal 76100, Melaka, Malaysia

ABSTRACT: Circularly polarized (CP) antennas minimize polarization losses and improve signal reliability in ultra-reliable and low-latency satellite communication. Compact design, wide impedance, and axial ratio bandwidth (ARBW) are key requirements for circularly polarized antennas utilized for modern automotive wireless applications. In this work, a miniaturized slotted antenna for C-band automotive-oriented wireless applications is proposed. The antenna achieves a wide measured impedance bandwidth of 69.5% (4.0–8.26 GHz, 4.26 GHz) and exhibits an ARBW of 51% (4.96–8.33 GHz, 3.37 GHz). The overall compact size of $25 \times 30 \times 1.6\,\text{mm}^3$ ($0.33\lambda \times 0.40\lambda \times 0.02\lambda$ at 4 GHz) further underscores its suitability for integration in space-constrained C-band communication systems. The anticipated design is optimized using rigorous parametric analysis to achieve a wide ARBW from $\theta = -27^\circ$ to $+33^\circ$ which is very beneficial for satellite applications. The fabricated prototype demonstrates a measured peak gain of 4.8 dBi and radiation efficiency ranging from 82% to 92% across the radiating band. Measurement results obtained from the fabricated antenna are validated with simulations and show satisfactory agreement. The anticipated design, compared with existing literature, is found to outperform other designs in terms of size, ARBW, and impedance bandwidth. The achieved resonance in the proposed design can be utilized for satellite communication, medical and automotive applications (tele-operated driving support, high-definition map collecting and sharing, infrastructure-based teleoperated driving), and other applications in C-band.

1. INTRODUCTION

Circularly polarized (CP) antennas are extensively used in wireless communication due to their ability to predict polarization mismatch and flexibility of alignment angle between transmitting and receiving antennas [1]. Apart from these features, CP antennas also offer high gain, improved radiation performances, and resilience to multipath fading which makes them a suitable candidate for ultra-reliable and low-latency satellite communication in automotive applications [2]. Achieving broadband impedance bandwidth and ARBW along with a compact, low-profile, light design is crucial and challenging for CP antennas utilized in these applications [3]. CP radiations are produced by superimposing two orthogonal electric fields with the equivalent amplitude and in 90° phase quadrature [4]. A conventional and well-known method to achieve CP radiation in planar antennas is by using truncated slots on the patch thereby exciting the orthogonal modes [5].

However, these conventional methods result in poor impedance and axial ratio bandwidths and are unsuitable for satellite-oriented automotive applications. For instance, in [6] a co-planar waveguide (CPW)-fed slot antenna with wideband CP is proposed. The design achieves an 87.8% impedance bandwidth and a 73.05% ARBW by incorporating structural modifications by introducing an L-shaped strip, square stubs, and peripheral slots. In a similar design, a miniaturized CP antenna for radio-frequency identification (RFID) applications is proposed [4]. The antenna design has an L-shaped feedline and stubs and achieves a wide ARBW of 460 MHz (818–1278 MHz) and a 54.6% impedance bandwidth (630–1103 MHz). Further, in [7], the concept of a triple-wideband three band CP equal sided slot antenna is projected featuring an L-shaped radiator and rectangular strips. The antenna achieves bandwidths of 1.32 GHz and 5 GHz with ARBWs for triple bands at 35.9%, 44.0%, and 6.3% suitable for C- and X-band applications. Thereafter, the authors in [8] demonstrated a slot antenna intended for C-band applications. The antenna achieves wide impedance and ARBW through a microstrip-fed structure with a protruded stub. The compact design ($25 \times 25\,\text{mm}^2$) offers a bandwidth of 90.2% (3.5–9.25 GHz) and a 40% ARBW (4.6–6.9 GHz), making it suitable for applications like WLAN and WiMAX.

The researchers in [9] projected a compact, microstrip fed, inverted L-shaped CP antenna designed for C-band use

* Corresponding author: Ahmed Jamal Abdullah Al-Gburi (ahmedjamal@ieee.org).

cases. The design achieves a wide bandwidth of 50.9% (3.48–5.86 GHz) and a 3 dB ARBW of 16.2% (4.71–5.54 GHz) using stub-matching and defected ground structures. The antenna offers a maximum gain of 5.32 dBi, making it appropriate for C-band downlink frequencies and other wireless applications. Apart from these methods, researchers have proposed using sequential rotation in antenna arrays [10–13] which results in increased system size, or using a slotted circular patch design [14–18]. In [14], the authors presented a compact 2×2 CP antenna array operating at 2.45 GHz, designed for energy harvesting. It features unbalanced slots on a circular patch for compactness and improved circular polarization. The 2×2 array achieves a gain of 10.8 dBi, a 3 dB ARBW of 140 MHz, and a lowest axial ratio of 0.15 dB, with a rectifier circuit enabling voltage multiplication for enhanced energy conversion. In a similar design [15], the authors presented a CP-slotted patch antenna designed for radio frequency (RF) power scavenging applications. It features a compact structure, optimized for high gain (> 6.0 dBic) and a 3-dB ARBW (2.36 GHz–2.40 GHz), making it suitable for efficiently converting scattered electromagnetic waves into electrical energy. The authors in [16] discuss the design of a wideband CP antenna array featuring sequentially rotated feed technology. It achieves a wide bandwidth (4.62–9.92 GHz) and ARBW (4.48–8.52 GHz) with a miniaturized structure and a maximum gain of 7.5 dBi, making it appropriate for modern wireless communications. Further, a miniaturized 4×4 CP antenna array is proposed for next-generation small satellites in [17]. The design uses a sequential phase feed structure to enhance gain, bandwidth, and axial ratio performance while preserving a compact size. The antenna achieves a left-handed CP gain of over 12 dBic with an AR below 1.5 dB across an operating bandwidth of 8.05 to 8.25 GHz. In a similar research paper [18], metasurface has been utilized along with the sequential feeding structure, and the authors propose a single-layer, wideband CP 2×2 antenna arrays for C-band wireless use cases. The antenna design uses a chamfered corner patch and intermittent metallic plates to attain a wide operating bandwidth of 2 GHz with a high gain ranging from 9.5 to 11.5 dBic.

It is evident from the literature survey that although various methods are proposed to achieve CP in planar antennas, a narrow ARBW of the order of a few MHz poses a major challenge in implementing practical automotive applications. Some literature proposes antenna arrays for enhancing the gain and ARBW of CP antennas. However, it increases the total extent of the antenna. To the best of our knowledge, wide impedance bandwidth and ARBW have not been achieved with a miniaturized single-element antenna. Motivated by this, this paper proposes a miniaturized slotted antenna for C-band satellite-oriented automotive applications. The proposed antenna is appropriate for ultra-reliable, low-latency satellite communication for automotive applications, and has ultra-wideband (UWB) impedance bandwidth, and broad ARBW in the frequency band of sub-6 GHz. The wide ARBW facilitates the antenna to be free from polarization losses and maintain reliable and uninterrupted transmission in the case of satellite communications. The key features like miniaturized size ($25 \times 30 \times 1.6\,\text{mm}^3$), wide ARBW ($\approx 3.72$ GHz) and impedance bandwidth (≈ 4.63 GHz) of the anticipated antenna make it suitable for C-band automotive and satellite applications.

2. ANTENNA DESIGN CONSIDERATIONS

The proposed design is fabricated on an FR4 substrate with $\varepsilon_r = 4.4$, $h = 1.6$ mm and loss tangent $= 0.02$. The design steps to reach the final stage of the proposed design are listed below:

- **Step-1:** A rectangular-shaped slot is imprinted out from the ground plane and is excited with the feedline as shown in Fig. 1(a). This initial design is a linearly polarized antenna.
- **Step-2:** Two side rectangular stubs are added in the feedline which generates two orthogonal modes with the same amplitude around 5.8 GHz. The dimensions of these stubs are optimized to improve the 3-dB axial ratio. However, a narrow 3-dB ARBW is achieved in this step.
- **Step-3**: Three slot strips are etched out in the ground plane to improve the axial ratio purity and ARBW as illustrated in Fig. 1(b).
- **Step-4:** The hexagon-shaped slot in the ground plane is partially covered from (b) and (c) to achieve maximum ARBW. The optimized antenna design after Step-4 is shown in Fig. 1(d).

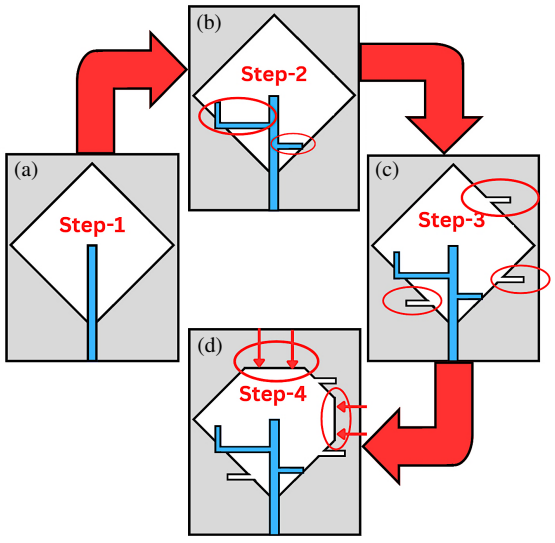

FIGURE 1. Various steps for the proposed antenna design: (a) Step-1, (b) Step-2, (c) Step-3, and (d) Step-4.

The performance of antenna design in terms of return loss and axial ratio variation with frequency for Steps 1–4 is shown in Fig. 2. The axial ratio versus frequency plot for Steps 2–4 is presented in Fig. 2(a). It can be visualized from Fig. 2(a) that the design of Step 2 achieves the ARBW of 1.6 GHz, which improves to 2.6 GHz in Step 3. There is an improvement of 62.5% in ARBW with Step 3 as compared to the de-

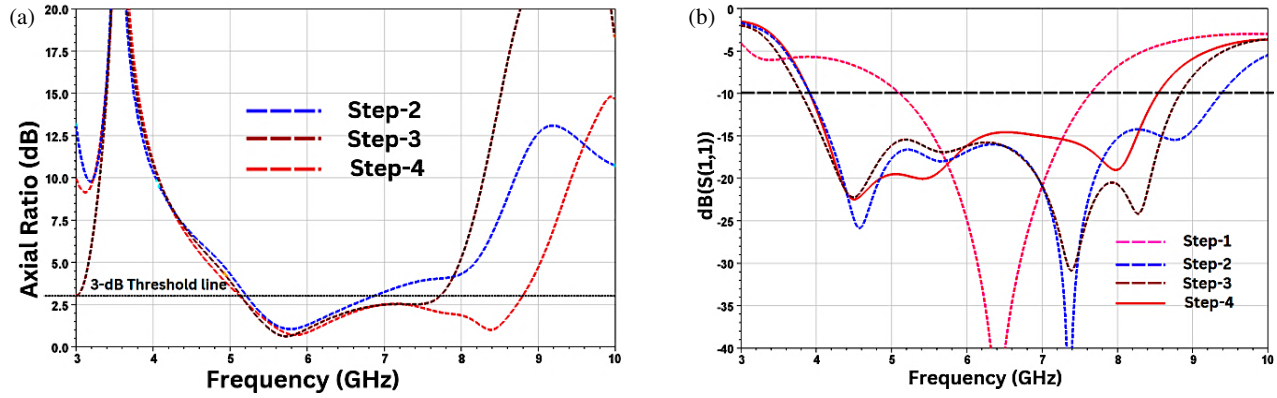

FIGURE 2. Step-wise variation in (a) axial ratio, (b) return loss S_{11} (dB).

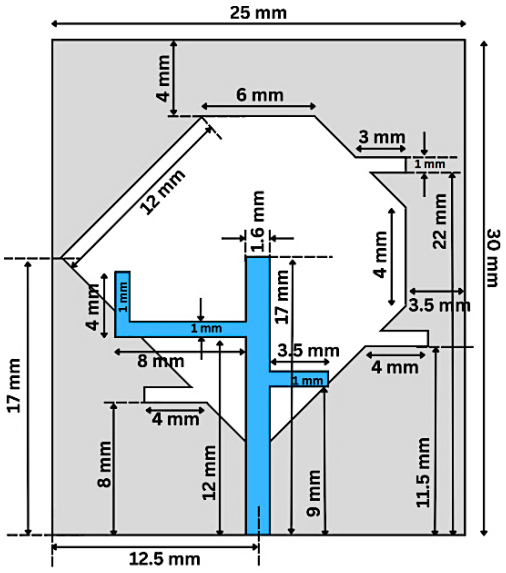

FIGURE 3. Dimensional parameters of the proposed design.

sign presented in Step 2. Finally, the proposed optimized antenna designed in Step 4 achieves the overall wide band ARBW $\approx$ 3.72 GHz. Similarly, the reflection coefficient (S_{11}) variations can be visualized in Fig. 2(b), which depicts the minimum bandwidth in Step 1. However, the bandwidth is widened in Step 2 but the ARBW is not much enhanced in Step 2. Therefore, an optimized sufficient impedance bandwidth and ARBW have been achieved in the final proposed design, i.e., Step 4. The illustration of the anticipated design is presented in Fig. 3, which demonstrates its compactness in terms of size (only 25 mm $\times$ 30 mm $\times$ 1.6 mm).

3. CURRENT DISTRIBUTION

The current distribution of the anticipated design at all the resonating frequencies is shown in Fig. 4. It can be visualized from Fig. 4 that different stubs that are cut in the ground plane are responsible for the excellent impedance matching in the wide frequency band. For a very low frequency band of operation, the left side of the design exhibits a significant portion of the current. Similarly, the right portion of the design exhibits current density which causes the impedance matching for a higher band of frequencies. Moreover, the design exhibits wide band ARBW, i.e., right-hand circular polarization (RHCP) demonstrating the vector current density at different phases for 6 GHz as shown in Fig. 5. Further, it can be visualized from Fig. 5 that the E-field vector interchanges anti-clockwise suggesting that the antenna delivers RHCP.

4. PARAMETRIC ANALYSIS

This section presents a comprehensive parametric analysis undertaken on the dimensional specifications of the proposed antenna design to achieve optimized impedance bandwidth and ARBW. It includes studying the effect of (A) the diagonal length of polygon, the variation of axial ratio with (B) the length of top cover, (C) the length of side cover, and (D) the length of upper right stub and lower left stub. For instance, Fig. 6(a) depicts the alteration of S_{11} with the change in dimensions of the polygon's diagonal length (D). It can be visualized from Fig. 6(a) that each 1 mm increment improves the impedance bandwidth significantly. Finally, $D = 24$ mm is chosen as the optimal value for the diagonal length of the polygon. It is to be noted that a further increase in the diagonal length shifts the operating band and hence is neglected in this analysis. Next, Fig. 6(b) depicts the length of top cover (L) of the hexagonal slot in ground plane. This dimension directly impacts the ARBW as illustrated in Fig. 6(b). The results were captured by varying length L from 3.9 mm to 4.5 mm. The highest ARBW is achieved with the value of $L = 4$ mm which is chosen as optimal value. Further, the variation of axial ratio with length of side cover (S) can be visualised in Fig. 6(c). It can be visualized from Fig. 6(c) that ARBW remains almost the same for $S = 3.0$, 3.3 & 3.7 mm. However, the highest ARBW has been achieved with $S = 3.5$ mm and is therefore chosen as the optimized value for the side cover. At last, another parameter of interest is the length of stubs as shown in Fig. 6(d) which depicts a variation of ARBW with a change in dimensions of the upper right-side slot (marked as A). The length of the slot ranges from 2 mm to 3.5 mm. Optimal ARBW is obtained at $A = 3$ mm as illustrated in Fig. 6(d). Similarly, dimension B is optimized from 3 to 5 mm and finally, $B = 4$ mm is selected as the optimized value achieving the highest ARBW as depicted in Fig. 6(e).

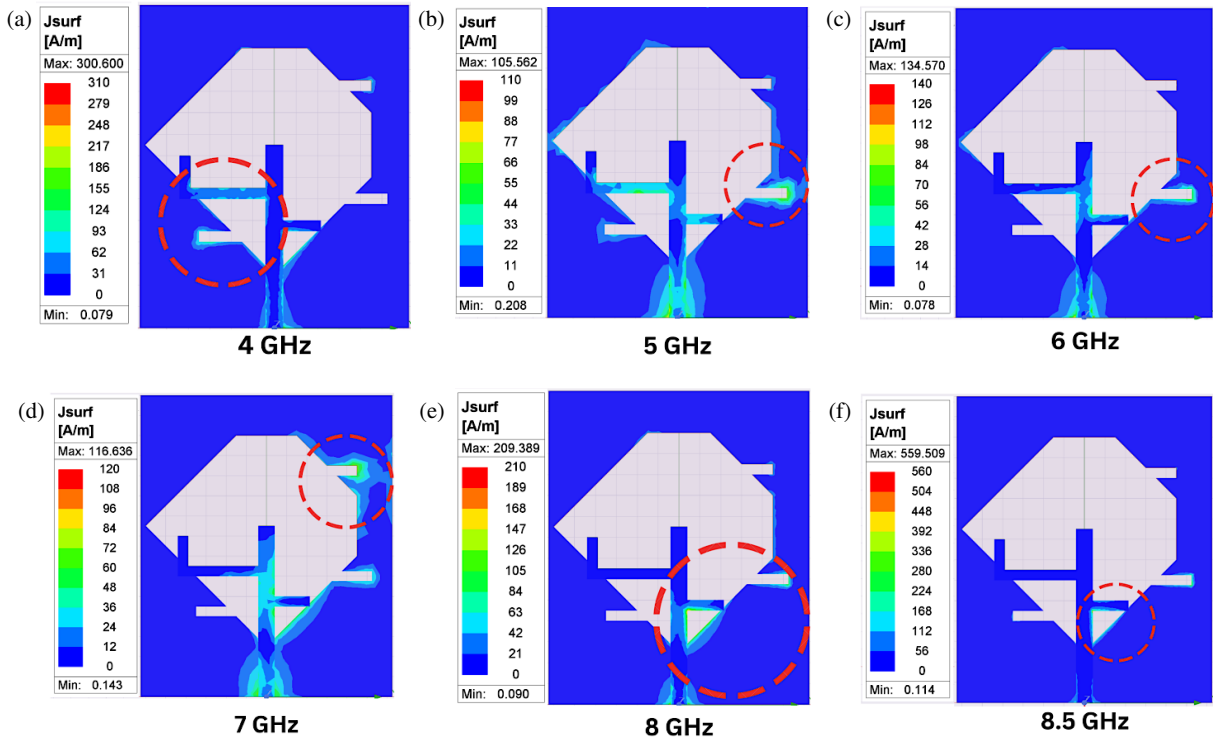

FIGURE 4. Current distribution of the proposed design at different frequencies.

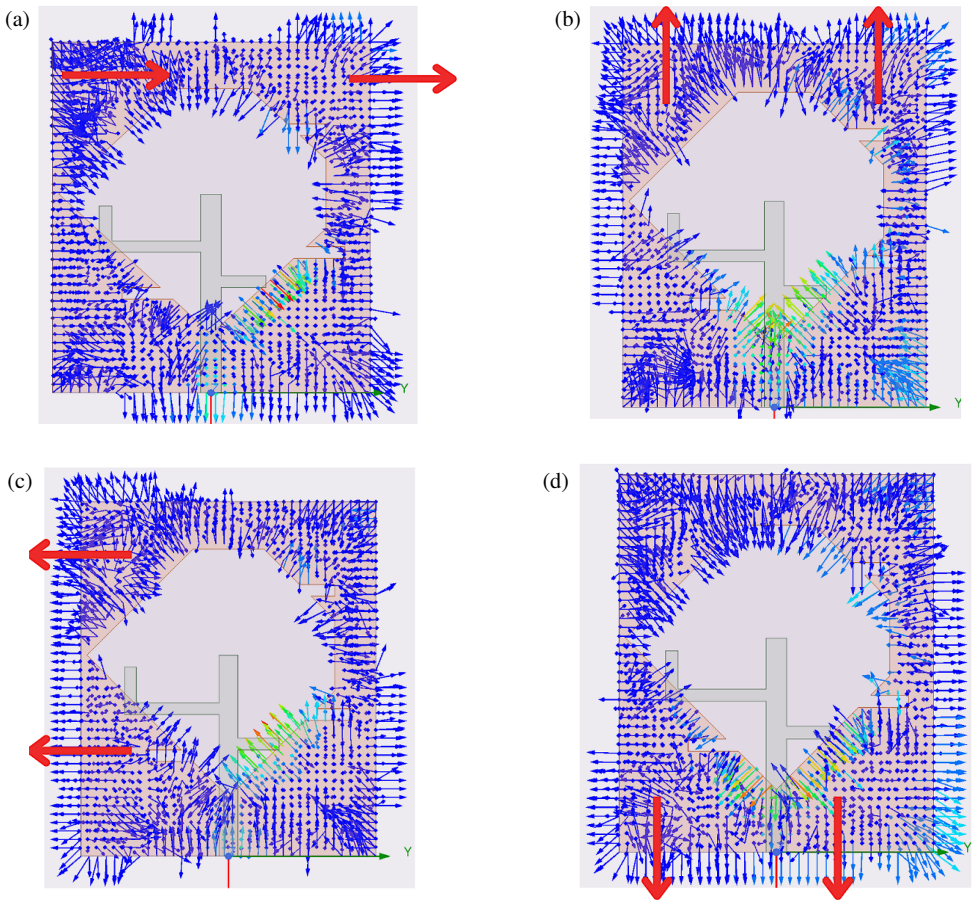

FIGURE 5. E-field vector at (a) 0°, (b) 90°, (c) 180°, and (d) 270°.

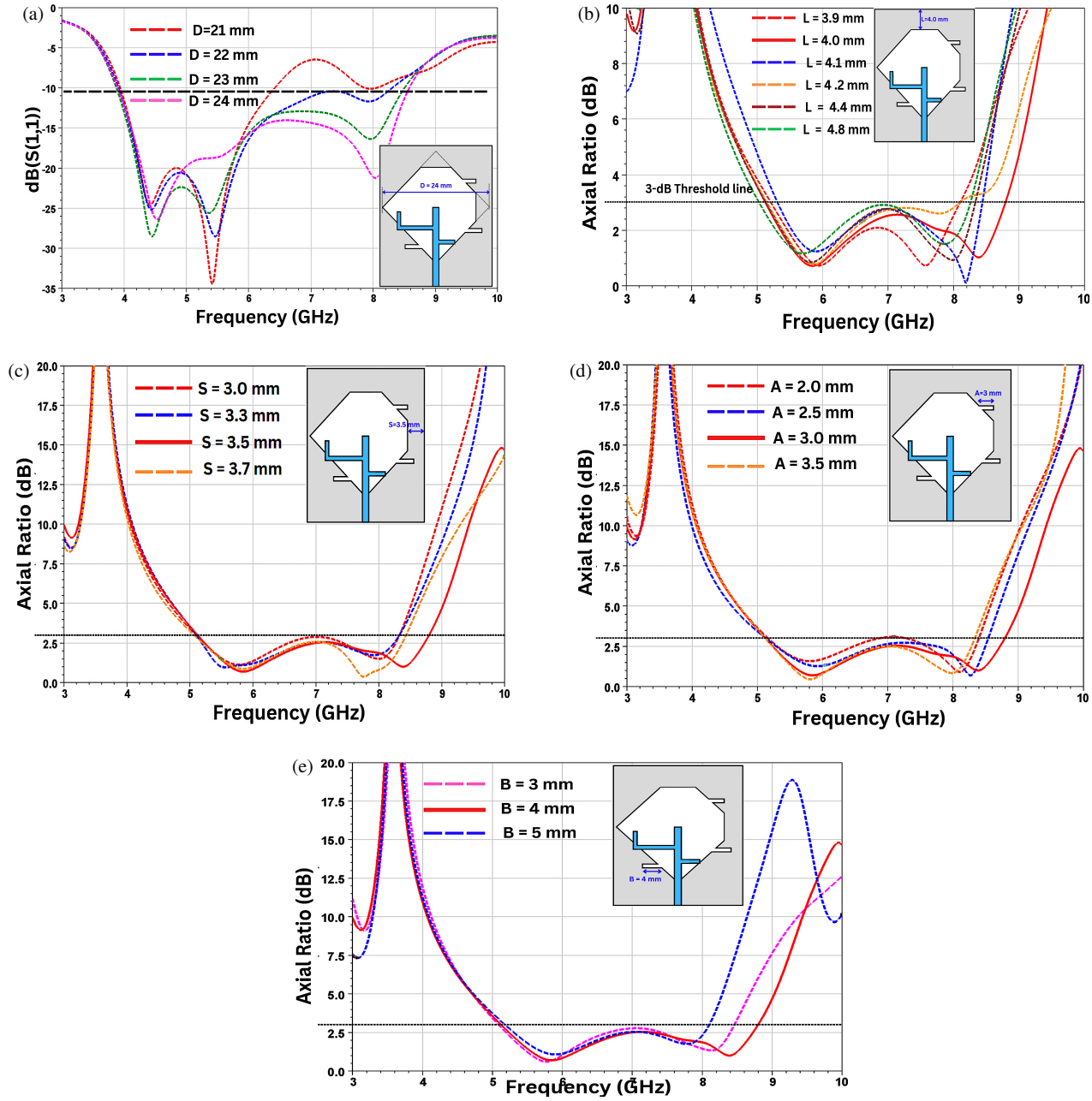

FIGURE 6. (a) S_{11} v/s frequency with variation in the diagonal length of the polygon (D); (b) Variation of ARBW w.r.t L for different frequency bands; (c) Axial ratio v/s frequency with variation in the length of side cover (S); (d) Variation of ARBW w.r.t A; (e) Variation of ARBW w.r.t B. The pictorial view of antenna elements is shown in a subset of each figure.

5. RESULTS AND DISCUSSIONS

The UWB capability of the anticipated antenna is illustrated in Fig. 7 using a return loss v/s frequency (GHz) plot. A bandwidth of 4.63 GHz is achieved as shown in Fig. 7. Further, the 3-dB AR of the optimized antenna design proposed in this work is demonstrated in Fig. 8. It can be visualized from Fig. 8 that an ARBW of 3.72 GHz is achieved with this design. The axial ratio graph presented in Fig. 9 shows polarization in the broadside direction. However, in the case of CP antennas, it is more significant that the antenna provides CP radiations not only in broadside direction but also away from it. Therefore, Fig. 9 demonstrates the axial ratio variations at different theta angles, which depicts that the antenna exhibits CP characteristics from $-27°$ to $+33°$ in the same frequency band. The overall analysis of Fig. 9 shows that the proposed antenna has minimum polarization losses in the frequency band of interest.

6. FABRICATION AND MEASURED RESULTS

The simulation results for the antenna design are calculated on Ansys HFSS software which is further validated using measurement results from the fabricated sample of the antenna. The fabricated prototype of the anticipated design is shown in Fig. 10.

The performance characteristics of the fabricated prototype was experimentally measured using a Keysight P9372A vector

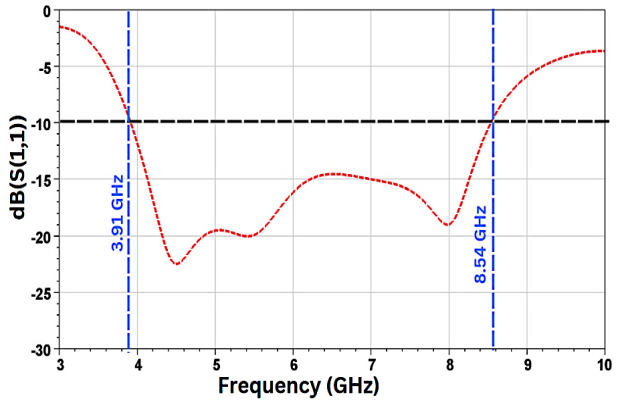

FIGURE 7. Return loss variation of the proposed design with frequency showcasing bandwidth from 3.91 GHz to 8.54 GHz.

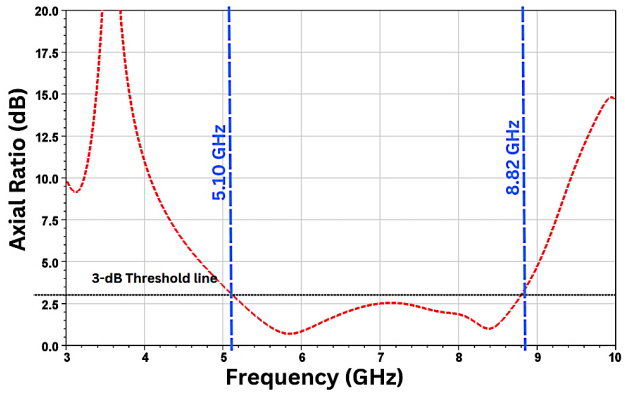

FIGURE 8. Axial ratio of the proposed antenna with frequency presenting a 3 dB axial ratio of 5.10 GHz–8.82 GHz.

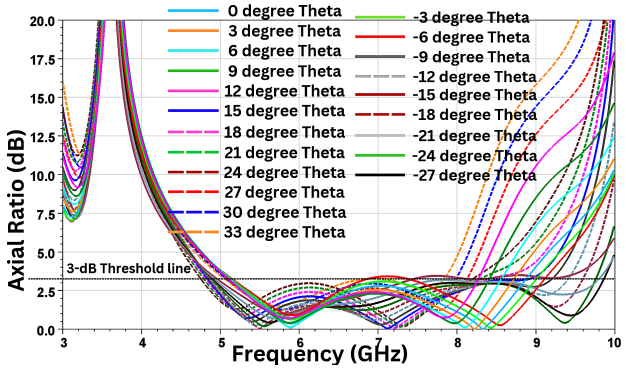

FIGURE 9. Axial ratio v/s frequency for different values of theta from -27 degree to $+33$ degree showcasing 3 dB BW.

network analyzer (VNA). All measurements were conducted inside an anechoic chamber with dimensions of 3 m $\times$ 3 m $\times$ 2.6 m, which provides a reflection-free environment for reliable antenna testing. The setup enabled accurate evaluation of the impedance bandwidth, radiation patterns, axial ratio, gain, and efficiency of the proposed antenna.

The comparative analysis of the proposed design's simulated and measured return losses in terms of S_{11} (dB) is visualized in Fig. 11 and demonstrates thier excellent agreement. The simulated curve covers the frequency range from 3.91 to 8.82 GHz (4.91 GHz), and measured results cover the bandwidth from 4 to 8.26 GHz (4.26 GHz). Although the measured bandwidth is marginally narrower, it still fully covers the band of interest (4–8 GHz), ensuring no compromise in performance for the intended C-band applications. The simulated S_{11} values remain in the -15 to -20 dB range across most of the operating frequencies, whereas the measured results predominantly exhibit return loss values better than -20 dB, confirming adequate impedance matching. The small offset can be attributed to fabrication tolerances, connector effects, and chamber measurement uncertainties, which are common in practical antenna prototypes. Overall, measured and simulated results are in good agreement, and the antenna maintains the required performance across the entire target frequency band. Further, the variations in gain are illustrated in Fig. 12 which demonstrates that the measured gain values are slightly less than the simulated results. The measured bandwidth and gain are less than the simulated bandwidth and gain because the simulations are performed in ideal boundary conditions. However, during fabrication and measurement, some parameters such as fabrication imperfections, material loss, environmental interactions, connector and feed network loss, very sharp edges in the proposed design, and impedance mismatch may impact the overall results.

Further, the axial ratio comparison is shown in Fig. 13 which depicts a wide ARBW in measured and simulated results. However, a better ARBW in measured results has been achieved at the cost of polarization purity near the 5.8 GHz–6.5 GHz frequency band. The value of the AR is very near the 3 dB in measured values. But still, the two curves are in good agreement. A wide measured 3-dB axial ratio (AR) bandwidth of 3.37 GHz, extending from 4.96 GHz to 8.33 GHz, is achieved, whereas the simulated ARBW spans 5.10–8.82 GHz (3.72 GHz). Although the measured ARBW is marginally reduced compared to simulation, it still covers more than 80% of the measured impedance bandwidth (4.00–8.26 GHz). More importantly, the measured ARBW fully encompasses the band of interest (4–8 GHz), thereby ensuring stable circular polarization across the operating frequencies. To further confirm the polarization purity and angular stability, axial ratio beamwidth analysis is carried out. The AR beamwidth defines the angular region over which the antenna maintains AR $\leq$ 3 dB, a key parameter for ensuring reliable circular polarization in satellite links. Fig. 14 illustrates the angular performance of the antenna at 6 GHz, presented as Cartesian plots of AR (dB) versus θ for $\varphi = 0°$ (E-plane) and $\varphi = 90°$ (H-plane). The measured results indicate that the antenna achieves a 3-dB AR beamwidth of approximately 67° in the $\varphi = 0°$ plane and 84° in the $\varphi = 90°$ plane. These values demonstrate that the proposed structure maintains circular polarization over a sufficiently wide angular region.

Next, the radiation pattern of the anticipated design at various resonating frequencies is shown in Fig. 15, which depicts the bidirectional nature of the radiation pattern. The simulated and measured radiation patterns show excellent agreement.

The measured and simulated radiation efficiencies of the proposed antenna are shown in Fig. 16. It can be observed that the radiation efficiency remains consistently high across the operating band of 4–8.26 GHz, with measured values ex-

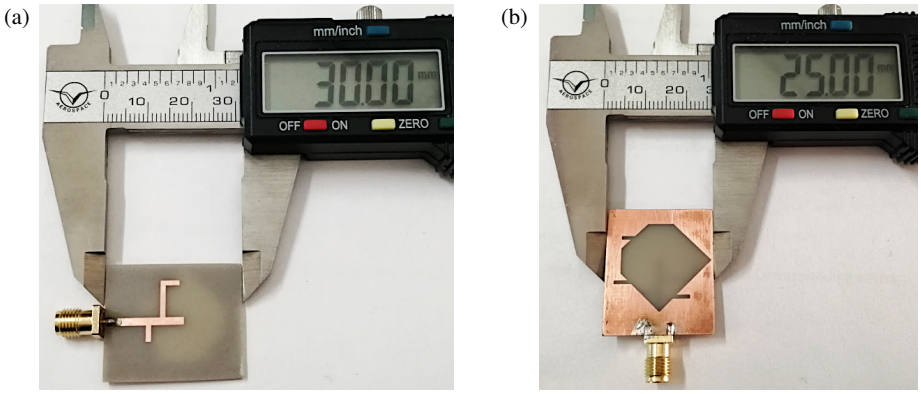

FIGURE 10. Fabricated prototype of the proposed design. (a) Feed plane, (b) ground plane.

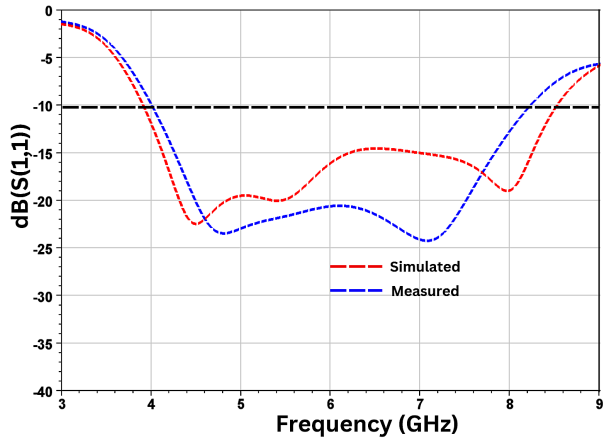

FIGURE 11. Comparative analysis of simulated and measured return losses of the proposed design.

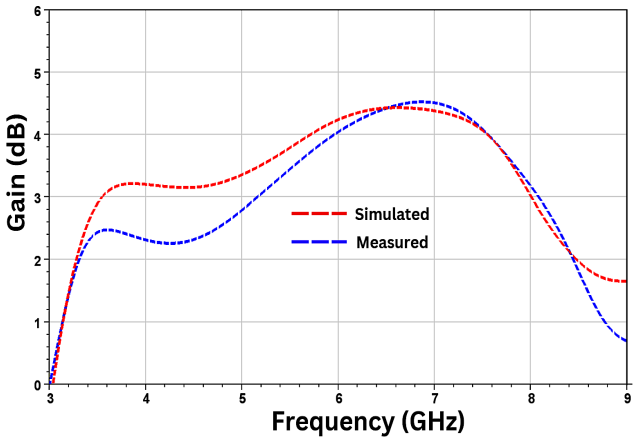

FIGURE 12. Comparative analysis of simulated and measured gains of the proposed design.

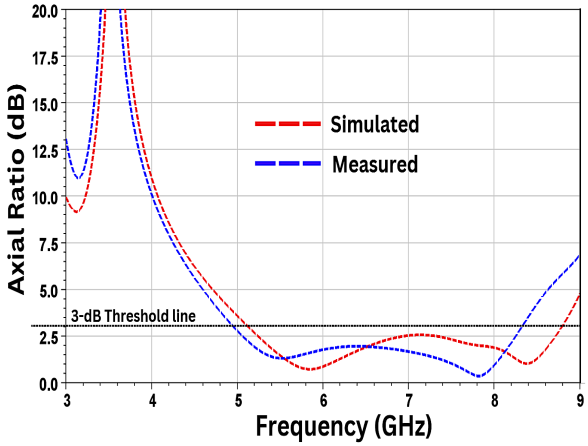

FIGURE 13. Comparative analysis of simulated and measured axial ratios of the proposed design.

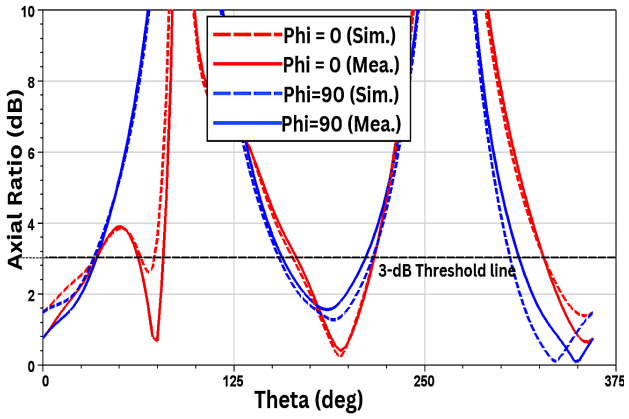

FIGURE 14. Axial ratio vs theta at 6 GHz.

ceeding 82%. The measured peak efficiency reaches approximately 92% at about 5.9 GHz, closely matching the simulated response, thereby validating the accuracy of the design model. This indicates that minimal power is lost due to dielectric or conductor losses, highlighting the effectiveness of the antenna design in ensuring efficient radiation, which confirms the suitability of the antenna for C-band satellite communication applications.

Further, the comparative analysis of the proposed design with the existing literature is shown in Table 1. The table describes the enhanced performance specifications of the anticipated design in comparison with other existing designs from the liter-

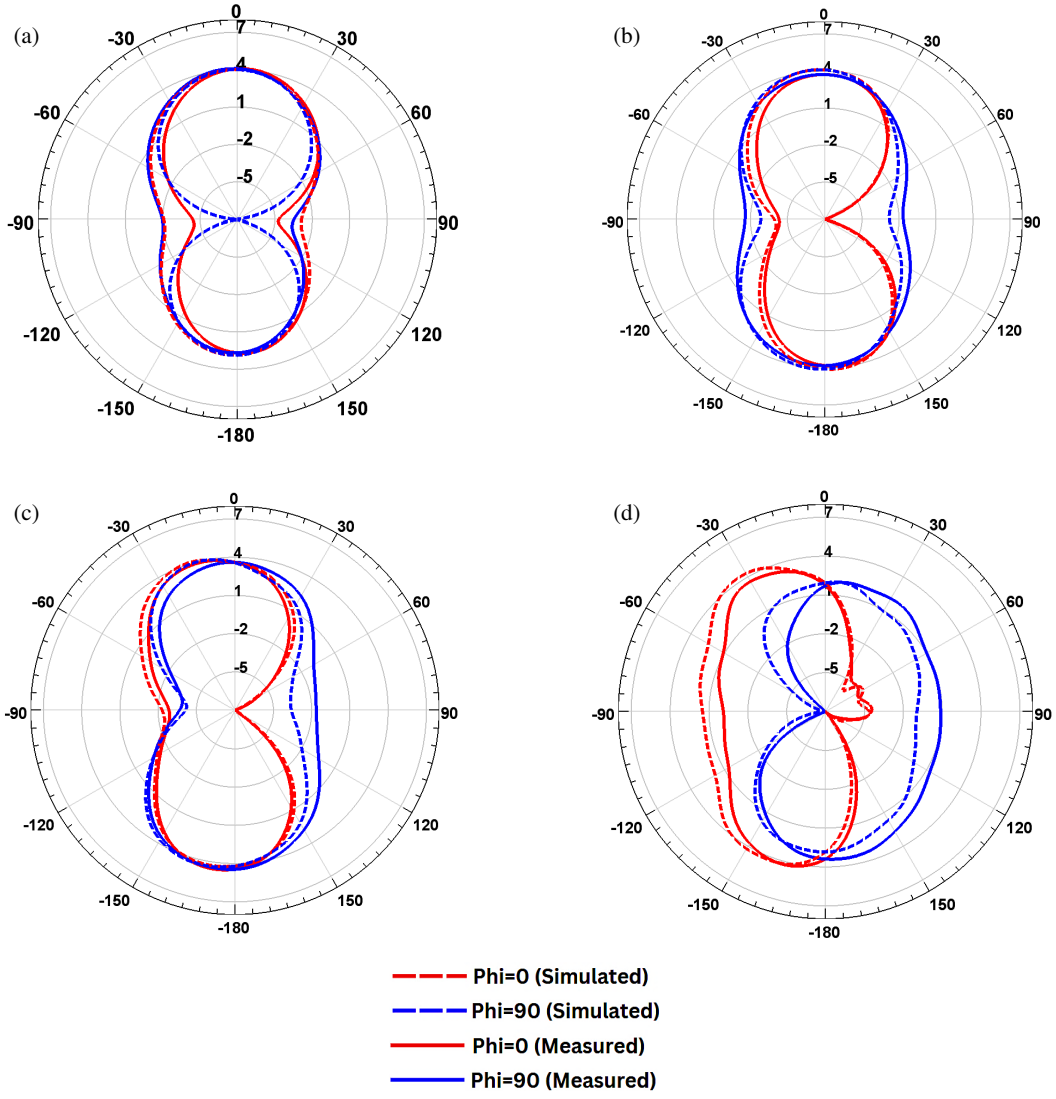

FIGURE 15. Radiation patterns at (a) 4 GHz, (b) 6 GHz, (c) 7 GHz, and (d) 8 GHz.

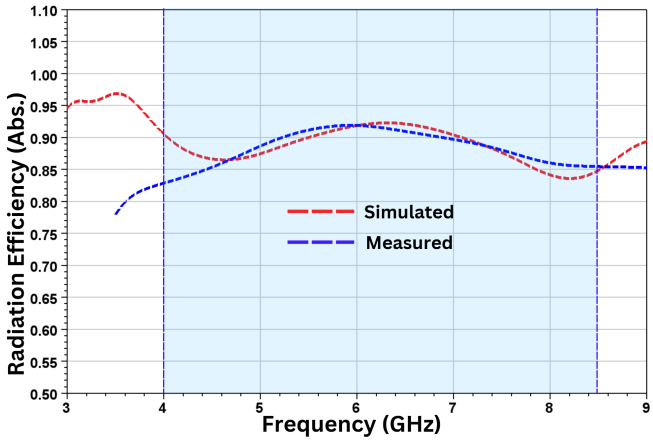

FIGURE 16. Radiation efficiency.

ature. It can be visualized from Table 1 that the proposed design outperforms the designs anticipated in the previous work in terms of −10 dB impedance bandwidth, size, and 3 dB ARBW. The proposed design has higher gain values than those presented in [7, 19, 20–24]. Although the gain of the proposed design is slightly lower than that reported in [9, 15, 16] but at

TABLE 1. Comparison of performance parameters of the proposed antenna with existing literature.

Ref.	Size (mm^3)	Relative Size	Operating Frequency Band (GHz)	−10 dB Impedance Bandwidth (%, MHz)	Gain (dBi)	3-dB ARBW (%, MHz)	Applications	Complexity & Cost
[19]	$120 \times 120 \times 1.6$	$0.25\lambda \times 0.25\lambda \times 0.003\lambda$	0.63–1.103	54.6% 473	4	43.9% 460	UHF RFID	Medium & low
[7]	$60 \times 60 \times 1$	$0.91\lambda \times 0.91\lambda \times 0.02\lambda$	4.55–9.55	70.9% 5000	4.2	6.3% 530	WLAN	High & low
[9]	$32 \times 32 \times 1.6$	$0.54\lambda \times 0.54\lambda \times 0.02\lambda$	3.48–5.86	50.9% 2380	5.35	16.2% 830	Downlink frequency of C-band	High and low
[20]	$32 \times 25 \times 1.575$	$0.59\lambda \times 0.46\lambda \times 0.03\lambda$	5.5–6.67	19.2% 1170	4	12.1% 760	Satellite Applications	Low & High
[15]	$60 \times 60 \times 3.2$	$0.46\lambda \times 0.46\lambda \times 0.02\lambda$	2.304–2.439	5.69% 135	6	1.68% 80	RF energy harvesting	High & low
[16]	$46 \times 46 \times 1.6$	$0.71\lambda \times 0.71\lambda \times 0.02\lambda$	4.62–9.92	72.9% 530	7.5	62.2% 4040	Modern Wireless Communications	High & low
[21]	$60 \times 60 \times 1.6$	$0.68\lambda \times 0.68\lambda$	2.2–2.47 3.42–3.54	11.6% (270) 3.5% (120)	3.43 2.09	33.63% (790) 4.20% (120)	Wi-Fi & MiMAX	High & Low
[22]	$31 \times 31 \times 1.6$	$0.29\lambda \times 0.29\lambda \times 0.02\lambda$	2.82–8.53	100.6% (5710)	4.47	N.A.	SHFB	Medium & low
[23]	$50 \times 50 \times 1.6$	$0.62\lambda \times 0.62\lambda \times 0.02\lambda$	3.2–4.4	31.57	4	N.A.	5G NR C-band	Low & Medium
[24]	$30 \times 40 \times 1.6$	$0.32\lambda \times 0.42\lambda \times 0.02\lambda$	3.2–5.85	43.98	3.5	N.A.	5G New Radio (NR) sub-6 GHz n77/n78/n79	High & Medium
Proposed design	$25 \times 30 \times 1.6$	$0.33\lambda \times 0.4\lambda \times 0.02\lambda$	4–8.26	69.5% 4260	4.8	51% 3370	C-band satellite applications	Low & low

the cost of the size. Moreover, the proposed design demonstrates a significantly smaller overall size than all the previously reported antennas cited in this section. It can be decided that the proposed design exhibits miniaturized size and wide impedance bandwidth and ARBW in comparison to existing literature, which is very suitable for ultra-reliable and low-latency satellite-oriented automotive applications.

7. CONCLUSION

This article presents a compact slotted patch antenna that features CP radiation with wide impedance bandwidth and ARBW. The proposed design has been optimized with rigorous parametric analysis by inserting stubs in the feed line and slotted ground structure to achieve the required performance parameters. The proposed design exhibits a measured impedance bandwidth of 69.5% (4.0–8.26 GHz, 4.26 GHz) and ARBW of 51% (4.96–8.33 GHz, 3.37 GHz) with a peak gain of 4.8 dBi. Additionally, the suggested design is manufactured, and the measured outcomes agree well with the simulated ones. The proposed design outperforms other existing antenna designs concerning various performance parameters. The covered frequency bands facilitate the proposed antenna design for C-band satellite-oriented automotive applications which offers minimized polarization losses and improved signal reliability in ultra-reliable and low-latency satellite communication.

ACKNOWLEDGEMENT

The authors would like to thank Universiti Teknikal Malaysia Melaka (UTeM), the Center of Research and Innovation Management (CRIM), and the Ministry of Higher Education (MOHE) of Malaysia for supporting this project.

REFERENCES

[1] Al-Gburi, A. J. A., Z. Zakaria, H. Alsariera, M. F. Akbar, I. M. Ibrahim, K. S. Ahmad, S. Ahmad, and S. S. Al-Bawri, "Broadband circular polarised printed antennas for indoor wireless communication systems: A comprehensive review," *Micromachines*, Vol. 13, No. 7, 1048, 2022.

[2] Darimireddy, N. K., R. Nalanagula, R. Kumari, D. Z. Mohammed, Z. Zakaria, and A. J. A. Al-Gburi, "Wideband circularly polarized inverted cup shaped hybrid dielectric-resonator antenna over an asymmetric jerusalem cross-based metasurface,"

Progress In Electromagnetics Research Letters, Vol. 125, 59–66, 2025.

[3] Wang, H., X. Lei, T.-D. Duan, T.-P. Li, M.-Y. Zhao, J. Gao, and P. Lu, "Circularly polarized waveguide aperture array antenna with a wide axial ratio bandwidth," *IEEE Antennas and Wireless Propagation Letters*, Vol. 21, No. 8, 1644–1648, 2022.

[4] Yadav, S. K., A. Gupta, V. Kumar, *et al.*, "Prediction of axial ratio using machine learning (ML) for a dual-band circularly polarized dielectric resonator antenna (DRA)," *Chinese Journal of Physics*, Vol. 96, 1364–1384, 2025.

[5] Midya, M., S. Bhattacharjee, G. K. Das, and M. Mitra, "Dual-band dual-polarized compact planar monopole antenna for wide axial ratio bandwidth application," *International Journal of RF and Microwave Computer-Aided Engineering*, Vol. 30, No. 5, e22152, 2020.

[6] Sharma, V. and T. Jhajharia, "Square slot antenna for wide circularly polarized bandwidth and axial ratio beamwidth," *Electrical, Control and Communication Engineering*, Vol. 17, No. 1, 1–11, 2021.

[7] Xu, R., J. Li, Y.-X. Qi, G. Yang, and J.-J. Yang, "A design of triple-wideband triple-sense circularly polarized square slot antenna," *IEEE Antennas and Wireless Propagation Letters*, Vol. 16, 1763–1766, 2017.

[8] Ellis, M. S., Z. Zhao, J. Wu, X. Ding, Z. Nie, and Q.-H. Liu, "A novel simple and compact microstrip-fed circularly polarized wide slot antenna with wide axial ratio bandwidth for C-band applications," *IEEE Transactions on Antennas and Propagation*, Vol. 64, No. 4, 1552–1555, 2016.

[9] Srivastava, K., B. Mishra, and R. Singh, "Microstrip-line-fed inverted L-shaped circularly polarized antenna for C-band applications," *International Journal of Microwave and Wireless Technologies*, Vol. 14, No. 4, 502–510, 2022.

[10] Evans, H., P. Gale, B. Aljibouri, E. G. Lim, E. Korolkeiwicz, and A. Sambell, "Application of simulated annealing to design of serial feed sequentially rotated 2×2 antenna array," *Electronics Letters*, Vol. 36, No. 24, 1987–1988, 2000.

[11] Ta, S. X. and I. Park, "Planar wideband circularly polarized metasurface-based antenna array," *Journal of Electromagnetic Waves and Applications*, Vol. 30, No. 12, 1620–1630, 2016.

[12] Ta, S. X. and I. Park, "Compact wideband circularly polarized patch antenna array using metasurface," *IEEE Antennas and Wireless Propagation Letters*, Vol. 16, 1932–1936, 2017.

[13] Zhang, Y., A. Chen, S. Cao, and D. Su, "Design of a circularly polarized 8×8 patch antenna array using a new series-parallel feed," in *2009 3rd IEEE International Symposium on Microwave, Antenna, Propagation and EMC Technologies for Wireless Communications*, 411–414, Beijing, China, 2009.

[14] Ong, C. S., M. F. Karim, L. C. Ong, T. M. Chiam, and A. Alphones, "A compact 2×2 circularly polarized antenna array for energy harvesting," in *2010 Asia-Pacific Microwave Conference*, 1977–1980, Yokohama, Japan, 2010.

[15] Jie, A. M., M. F. Karim, L. Bin, F. Chin, M. Ong, *et al.*, "A proximity-coupled circularly polarized slotted-circular patch antenna for RF energy harvesting applications," in *2016 IEEE Region 10 Conference (TENCON)*, 2027–2030, Singapore, 2016.

[16] Lu, Z., L. Yang, and L. Yang, "Design of a broadband circularly polarized antenna array," *Progress In Electromagnetics Research M*, Vol. 82, 195–203, 2019.

[17] Elahi, M., S. Trinh-Van, Y. Yang, K.-Y. Lee, and K.-C. Hwang, "Compact and high gain 4×4 circularly polarized microstrip patch antenna array for next generation small satellite," *Applied Sciences*, Vol. 11, No. 19, 8869, 2021.

[18] Srinivasan, K., M. Balasaraswathi, C. S. Boopathi, and H. H. Tran, "Single-layer wideband circularly polarized antenna array using sequential phase feed for C-band applications," *Wireless Networks*, Vol. 26, No. 6, 4163–4172, 2020.

[19] Ahmed, W. A. and Q. Feng, "A novel compact CP antenna with wide axial ratio bandwidth for worldwide UHF RFID handheld reader," *International Journal of Antennas and Propagation*, Vol. 2019, No. 1, 2497450, 2019.

[20] Ashraf, M. A., F. A. Tahir, and Q. H. Abbasi, "Circularly polarized C-shaped monopole antenna for C-band applications," in *2018 IEEE International Symposium on Antennas and Propagation & USNC/URSI National Radio Science Meeting*, 2389–2390, Boston, MA, USA, 2018.

[21] Thanki, P., T. Upadhyaya, U. Patel, K. Aliqab, M. Alsharari, A. A. Althuwayb, A. Armghan, and V. Sorathiya, "Dual band four port MIMO antenna with dual circular polarization for Wi-Fi/WiMAX applications," *Alexandria Engineering Journal*, Vol. 112, 1–16, 2025.

[22] Dkiouak, A., F. Rahmani, M. E. bakkali, N. E. Kamoun, M. Baghouri, and A. Zakriti, "A compact MIMO antenna with an equivalent circuit model for satellite communications, weather radar and 5G mobile technology," *Engineering Research Express*, Vol. 7, No. 3, 035344, 2025.

[23] Bose, M. and V. Karuppiah, "Metamaterial inspired superstrate loaded miniaturized quad port MIMO antenna for 5G C-band applications," *Optics Communications*, Vol. 574, 131123, 2025.

[24] Kulkarni, J., A. Desai, and C.-Y. D. Sim, "Wideband four-port MIMO antenna array with high isolation for future wireless systems," *AEU — International Journal of Electronics and Communications*, Vol. 128, 153507, 2021.